Three-terminal organic memory devices

Jun He, Liping Ma,[a] Jianhua Wu, and Yang Yang[b]
Department of Materials Science and Engineering, University of California at Los Angeles, Los Angeles, California 90095

(Received 15 September 2004; accepted 16 January 2005; published online 14 March 2005)

An organic electrical bistable device (OBD) has been reported previously, which has an organic/metal-nanocluster/organic structure sandwiched between a top and bottom electrode [L. P. Ma, J. Liu, and Y. Yang, Appl. Phys. Lett. **80**, 2997 (2002)]. This device can be switched between a low- (OFF) and a high- (ON) conductivity state by external bias. In this article, we report a three-terminal organic memory device, which is realized by wiring out the metal-nanocluster layer of the OBD as the middle electrode. The ON and OFF states of the device can be read out by measuring the potential of the middle electrode. By controlling the interface formation of the device, a three-terminal OBD with a potential change on the middle electrode of more than three orders in magnitude between the OFF state and ON state (from 0.2 mV to 0.77 V) is achieved. By wiring out the middle electrode, the three-terminal OBD can also be considered as two 2-terminal devices stacked together. By proper interface engineering (to be discussed in detail in the text), we found that both the top and bottom devices show electrical bistability and memory effect. This can double the data storage density of the memory device. Details of the device mechanism are provided. © *2005 American Institute of Physics*. [DOI: 10.1063/1.1866496]

I. INTRODUCTION

Organic memory devices are generally realized by interposing thin layers containing organic materials between two electrodes and have caused much attention[1–18] due to their potential advantages of flexibility, easy processing, low cost, and larger area fabrication by printing techniques. Generally, electrical bistability means there are two electrical states for a device, i.e., the high-conductance state (ON state) and the low-conductance state (OFF state), and the device can exist at either state for a prolonged time (retention time); under some applied condition, the device can be switched from one state to the other, which is ideal for rewritable nonvolatile memory application. Ferroelectric polymers have much lower permittivity and much slower switching speed than inorganic ferroelectrics,[2] which makes them less attractive for applications. On the other hand, significant research has been done on resistance switching since the 1970s. Initially, the focus was on organic thin-film memory in a charge-transfer complex system proposed by Potember and Pochler,[3] where the transition between the high-conductance state and low-conductance state is realized by charge transfer between copper and tetracyanoquinodimethane (TCNQ). The switching phenomenon was also observed in some polymer films,[4–6] and most of the earlier observed electrical memory effects turned out to be due to filament formation. Recently, Oyamada *et al.* demonstrated a switching effect in Cu:TCNQ charge-transfer-complex thin films, where a thin Al_2O_3 layer between the anode and the Cu:TCNQ layer is critical to the observed switching phenomenon.[7] Bandyopadhyay and Pal reported that conductance switching between three levels can be achieved in supramolecular structures of Rose Bengal,[8] where electroreduction and conformational change of the molecules cause the conjugation modification, and as a result, the conductance of the molecules is changed. Moller *et al.* demonstrated a write-once-read-many times memory by burning polymer fuses.[9,10] A high ON-state current memory device was reported by our research group, by controlling the copper ions within the organic layer.[11] The device structure is copper-anode/buffer-layer/organic-layer/cathode. The switching-on process is realized by applying a positive voltage pulse between the two electrodes, driving Cu^+ ions into the organic layer to transform the device into the high-conductance state. It is interesting to note that the Cu^+ can be expelled out of the organic layer by applying a higher-voltage pulse, which restores the device to the OFF state. This device is a rewritable nonvolatile memory device.

The memory device discussed in this manuscript is the organic electrical bistable device (OBD) with an organic/metal-nanocluster/organic trilayer structure sandwiched between two electrodes,[12–17] which shows nonvolatile memory behavior. The high-conductance state and the low-conductance state differ in their conductance by a factor as great as 10^6 and shows remarkable retention. Later, the switching and memory effect in OBD-structured devices have also been observed by the Campbell group.[18] It should be noted that their devices, although they also have the organic/nanoclusters/organic structure, are different from ours. First, they used a very thin (5 nm) Al-nanocluster layer, where the Al nanocluster should be a monolayer and resonant tunneling within the Al-nanocluster layer could not occur as it does in our device.[16,17] Second, their current–voltage (I–V) characteristics are different from ours. For their device, the ON state is restored to the OFF state at higher voltage, whereas for our devices reversed bias restores the device from the ON state to the OFF state. The Al nanoclus-

[a]Author to whom correspondence should be addressed; electronic mail: lma@ucla.edu
[b]Electronic mail: yangy@ucla.edu

ters in their devices may act as charge traps, i.e., charges are injected from the electrode, travel through the organic layer, and then are trapped by the Al nanoclusters, which is a process that may take time because carrier mobility in organic is very small. For our OBDs, we failed to observe the switching behavior when the Al-nanocluster layer is less than 10 nm (instead, we observed interesting current steps, not shown here), and the switching-on process is in nanoseconds, which cannot be explained in the charge injection-travel-and-trapped picture. Therefore, we believe that the mechanism for their device is different from ours.

All the above memory devices based on conductance change are detected by measuring the device current. From an application point of view, the memory cell should be as small as possible, such as in micrometer or submicrometer scale, in order to get a high density of data storage. In this case, the current through the memory cell may be too small to distinguish conveniently whether the device is in the ON state or OFF state. One way to solve this issue is to increase the ON-state current of the device by introducing Cu ions for ON state.[11] In this article, we discuss another approach to solve this issue by demonstrating a three-terminal OBD, which is realized by wiring out the metal-nanocluster layer of the OBD as the middle electrode. The ON and OFF states of the device can be read out by measuring the potential of the third terminal of a biased device, which is independent of the device area.

II. EXPERIMENT

The device fabrication processes are similar to what we previously reported.[13–15] The glass substrate is cleaned by a routine procedure. First, the glass substrates were sonicated in the order of detergent, de-ionized water, acetone, and isopropanol, and then baked in an oven at about 80 °C to prepare for fabrication. The OBDs are fabricated by thermal evaporation at 2.0×10^{-6} Torr. A substrate-moving system allows the deposition of each layer of the OBD without breaking the vacuum of the chamber. The organic compound and metal material we used are 2-amino-4,5-imidazoledicarbonitrile (AIDCN) and Al, respectively. At first, a 650-Å Al film was deposited on the precleaned glass substrate at a deposition rate of 3 Å/s for the bottom electrode, 400 Å of AIDCN film was deposited (0.5 Å/s) on it as the bottom organic layer, then 200 Å of Al and AIDCN mixed-film was deposited by coevaporation. The deposition rate of Al and AIDCN for the middle layer was 0.4 and 0.1 Å/s, respectively. Then another 400-Å AIDCN film at a deposition rate of 0.5 Å/s and an 800-Å Al film with a deposition rate of 2 Å/s were deposited sequentially to form the top organic and the top electrode layers. The overlap between the top and bottom electrodes is 0.4 mm^2, which is the size of OBDs mentioned in this paper. In order to study the potential distribution of the device, we wired out the metal-nanocluster layer during device fabrication by using shadow masks, where the dotlike metal-nanoclusterlayer is electrically connected to a predeposited Al strip as the third terminal. The purpose of the third terminal is for both the potential measurement of the nanoclusterlayer and also allows the voltage to be applied to any pair of the electrodes, testing the $I-V$ characteristics.

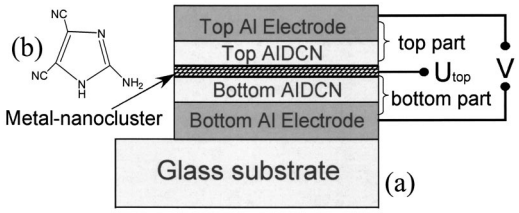

FIG. 1. (a) Device structure of the three-terminal OBD: the top electrode is grounded and bias is applied between the top electrode and the bottom electrode; the middle electrode is used for potential measurement; (b) the chemical structure of AIDCN.

The thickness of each layer was monitored by a quartz crystal calibrated with Dektak IIA. Current–voltage curves reported here were measured with a HP 4155B semiconductor parameter analyzer. The curves of the cyclic write-read-erase-read test and stress test were characterized by two Keithley 2400 Series Sourcemeters (one for applying the voltage cycles, the other for measuring the potential drop) controlled by a computer. All electrical measurements were done in ambient condition. The device structure of the three-terminal OBD is shown in Fig. 1(a). The chemical structure of the organic material used is shown in Fig. 1(b). Without specification, the top electrode is connected to the ground (0-V potential). The three-terminal OBD consists of the top part (top-electrode/top-organic/metal-nanocluster) and the bottom part (metal-nanocluster/bottom-organic/bottom-electrode). The resistance between the top electrode and the middle electrode is defined as R_{top} and the resistance between the bottom electrode and middle electrode is defined as R_{bottom}.

III. RESULTS AND DISCUSSION

The current–voltage ($I-V$) characteristic between the top and the bottom electrodes of a three-terminal OBD is shown in Fig. 2, which is similar to what we reported before.[12–17] During the first forward bias scan from −1.5 to 3 V, the device shows a very low current injection (negative bias is for

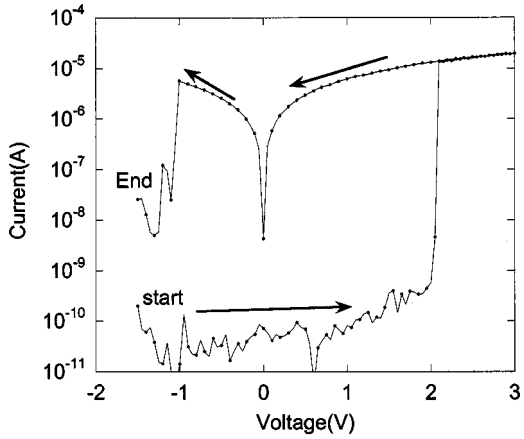

FIG. 2. The typical $I-V$ characteristics of a three-terminal OBD measured by top-bottom electrode. The nonzero current at $V=0$ V may be caused by the polarization of the nanocluster layer in the ON state.

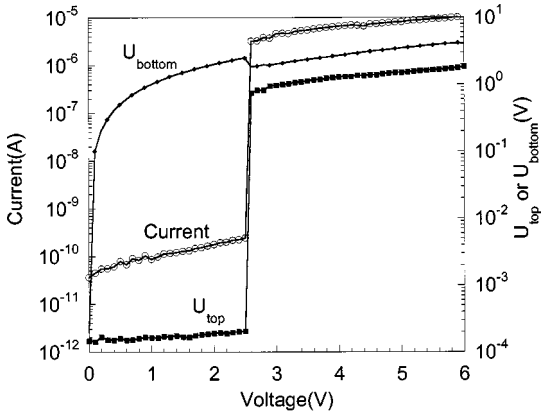

FIG. 3. The bias dependence of the potential drops on the top part (U_{top}) and the bottom part (U_{bottom}) of a three-terminal OBD (right *Y* axis) and the device current (left *Y* axis).

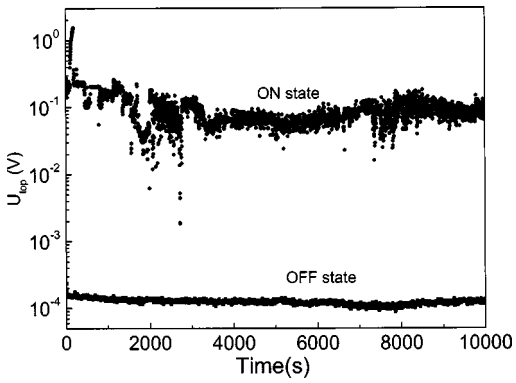

FIG. 4. Stress test of a three-terminal OBD in both the ON state and the OFF state. 1-V bias was applied between the top and bottom electrodes and U_{top} was read.

the purpose of making sure that the device is at the OFF state) until at a critical voltage (around 2 V here), where it switches from the OFF state to the ON state. As the bias is swept back from 3 to 0 V, the device remains in the ON state, indicating memory effect. As it is swept further to the negative voltage, the device was recovered to the OFF state at about −1 V, indicating rewritability of the device.

The readout of the three-terminal OBD is different from the previous two-terminal OBD. A low voltage, less than the switching voltage, is applied between the top and bottom electrodes, and the device state (ON or OFF) is read out by measuring the potential of the middle electrode. The write and erase process of the three-terminal device is the same as the two-terminal OBD. The beauty of the three-terminal OBD is that the potential change of the middle electrode is not a function of the device area, so the three-terminal OBD is not affected by the device area when the device area shrinks to micro- or submicro scale.

The potential drop between the top electrode and the middle electrode is defined as U_{top} and the potential drop across the bottom electrode and the middle electrode is defined as U_{bottom}. During the potential measurement, the top electrode of the device was grounded. Figure 3 shows the typical variation of the potential drop (U_{top} and U_{bottom}) with the applied voltage between the top and bottom electrodes for a three-terminal OBD initially at the OFF state. The current through the device was measured simultaneously as plotted by the left *Y* axis. It can be seen from Fig. 3 that for the device at the OFF state, the potential drop at the top part of the device is very small (around 0.2 mV) and at the switching-on voltage (here 2.5 V), U_{top} jumps by more than three orders in magnitude from 0.2 mV to 0.77 V. In the ON state, the potential drops between the top part and the bottom part of the device are comparable. In Fig. 3, we also plotted the curve for U_{bottom} by a simple calculation ($U_{bottom}=V-U_{top}$), showing that most of the applied potential is dropped in the bottom part of the device when it is at the OFF state. It should be mentioned that the resistance of the middle electrode (in kilohm range) is much smaller than the input impedance of HP4155B (1 GΩ). Therefore, the reading of U_{top} and U_{bottom} is reliable.

In order to study the retention time of the three-terminal OBDs for both the ON and OFF states, a small constant voltage (1 V) was applied between the top and bottom electrodes. The U_{top} is recorded to monitor the state of the OBD as shown in Fig. 4. In Fig. 4, the U_{top} for the ON state is three orders of magnitude higher than that of the OFF state. It can be seen from Fig. 3 that there is no significant degradation of the device in either the ON or OFF state during the 3-h stress test, indicating that both states are relatively stable. It should be noted that in Fig. 4 the OFF-state potential is quite smooth, while the ON-state potential shows some fluctuation, which may be caused by the charges stored in the Al nanoclusters when the device is at the ON state. Details about these fluctuations are under study.

The write-read-erase cycle test for a three-terminal OBD is shown in Fig. 5. The voltages for write, erase, and read are 2.5, −1.5, and 1 V, respectively. The ratio of U_{top} in the ON and OFF states is about 10^3 during the test. At the beginning of the cycle test [Fig. 5(a)], the success ratio of the programming was almost 100%. After 21 h of continual-cycle testing [Fig. 5(b)], the device still worked well and the ratio was still near 100%, but U_{top} at the OFF state increased by 1.5 orders from 0.1 to 10 mV, indicating device degradation. Two possible reasons are AIDCN recrystallization in air (not shown here) and oxidization of the interfaces of the device, causing the interface contact change. Details about the device degradation mechanism are under study. It should be noted that the time scale used in Fig. 5 is due to the inherent limitation of the test instrument and program.

Using the measured current and the U_{top} and U_{bottom} shown in Fig. 3, we derived the R_{top} and the R_{bottom} as shown in Fig. 6, from which one can see that both the R_{top} and R_{bottom} show switching behavior, but at the OFF state R_{bottom} is much larger than R_{top}. Since the nominal structure of the two parts of the three-terminal OBD is the same, a possible reason is that the interfaces of the top and bottom parts of the device are different. The interfacial roughness for both the top-Al/top-AIDCN and bottom-AIDCN/bottom-Al has been studied by using an atomic force microscope (AFM). The roughness of the top-Al/top-AIDCN interface should be determined by the surface roughness of the AIDCN layer, while the roughness of the bottom-AIDCN/bottom-Al interface should be dominated by the surface of the bottom Al layer. However, we found that the roughness of the two interfaces

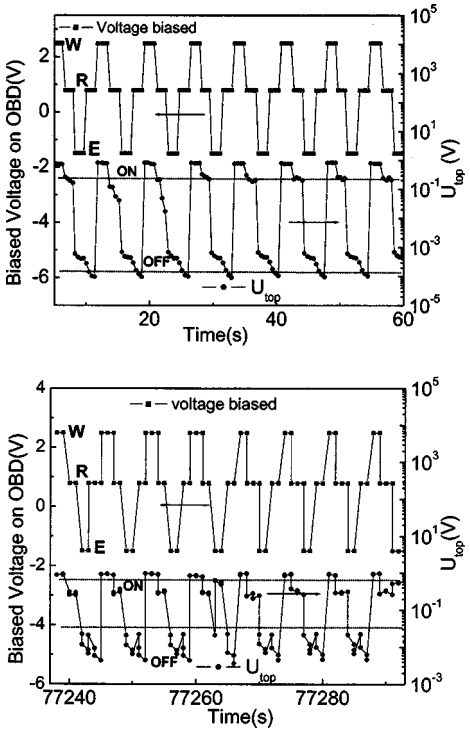

FIG. 5. Cyclic write-read-erase-read test of a three-terminal OBD. The upper curve is the voltage biased on the device and the bottom curve is the potential drop on the top part of the device. The voltages for write, erase, and read are 2.5, −1.5, and 1 V, respectively. In order to use a logarithmic axis for the potential drop across the top AIDCN layer, the current for the erasing process is an absolute value. (a) At the beginning of the cyclic test; (b) after 21 h of continual testing.

is comparable as shown by the AFM images [Figs. 7(a) and 7(b)] and section analysis [Figs. 7(c) and 7(d)] of the surface of the AIDCN film and the Al film, although the section analysis of the surface of the AIDCN film [Fig. 7(c), peak-peak vertical distance ~9.7 nm] is a little bit rougher than the Al film [Fig. 7(d), peak-peak vertical distance ~8 nm]. Therefore, the interfacial roughness may not be the main reason for the asymmetric potential distribution of the device, although the Al clusters may have some penetration into the top AIDCN layer when the top Al electrode was deposited.

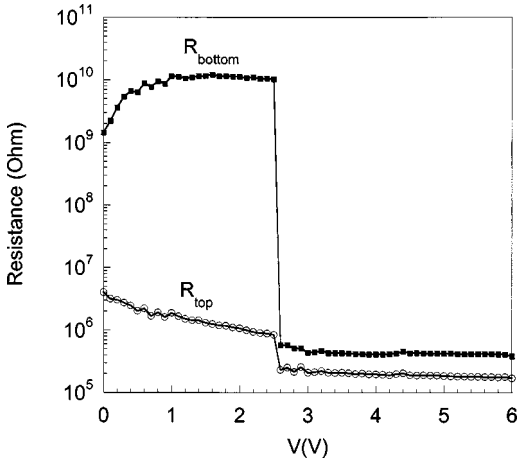

FIG. 6. The bias dependence of the resistance for both the top part and the bottom part of the three-terminal OBD, calculated from Fig. 3.

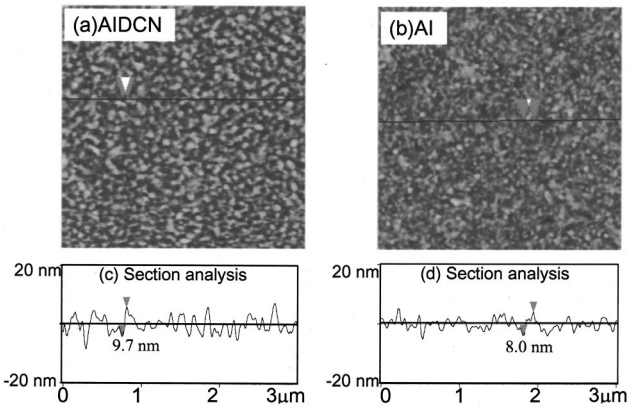

FIG. 7. The AFM images and sectional roughness analysis (along the line shown in the AFM images) for the surface of an AIDCN film and Al film. (a) The AFM image of the AIDCN surface, (b) the AFM image of the Al surface, (c) the sectional roughness analysis of the AIDCN film, and (d) the sectional roughness analysis of the Al film.

Another possible reason is that the degree of chemical reaction between the two interfaces is different, which is more probable for the devices. For the top-Al/top-AIDCN interface hot Al atoms are deposited onto the AIDCN surface, while for the bottom-AIDCN/bottom-Al interface, it is not-hot AIDCN molecules deposited on cold Al surface. As a result, chemical reactions between Al and AIDCN are likely to happen at the top-Al/top-AIDCN interface rather than at the bottom-AIDCN/bottom-Al interface. This assumption has been partially proven by the UV-visible absorbance spectra as shown in Fig. 8. Figure 8 shows the UV-visible absorbance spectra of a single AIDCN layer (40 nm), an Al (12 nm) deposited on top of an AIDCN (40 nm) film, and an AIDCN (40 nm) deposited on top of an Al (12 nm) film. All the films were deposited on a CaF_2 substrate with very small absorption in the UV-visible range. It can be seen from Fig. 8 that the UV-visible absorbance spectrum of a single AIDCN film shows a clear absorption edge at 350-nm wavelength, which is corresponding to the energy band gap of AIDCN (3.6 eV). The spectrum of AIDCN deposited on top of Al is similar to that of single AIDCN film, except for the significant base line increase caused by the Al layer. Therefore, there is no obvious chemical reaction at the bottom-Al/

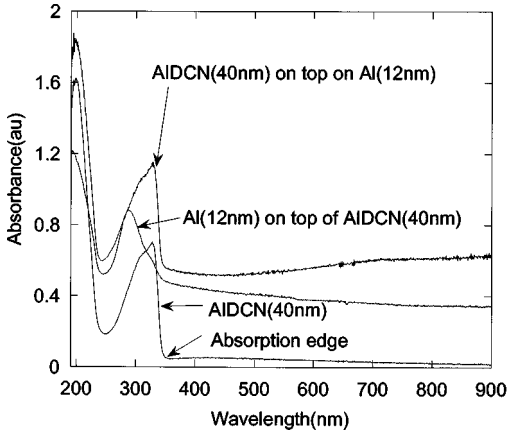

FIG. 8. UV-visible absorption spectrum for an AIDCN film, Al deposited on top of AIDCN film, and AIDCN deposited on top of Al film.

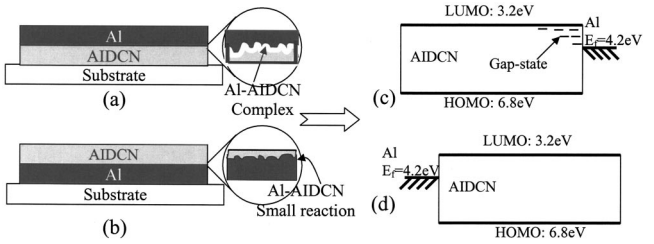

FIG. 9. Schematic diagram for the two interfaces of the top-Al/top-AIDCN and the bottom-AIDCN/bottom-Al. (a) Hot-Al deposited on top of the AIDCN surface, resulting in chemical reaction at this interface; (b) AIDCN deposited on cold-Al surface, resulting in small reaction; (c) band diagram for the top-Al/top-AIDCN contact, with band-gap state formation resulting in a relatively efficient electron injection; and (d) band diagram for the bottom-AIDCN/bottom-Al contact, with less efficient charge injection.

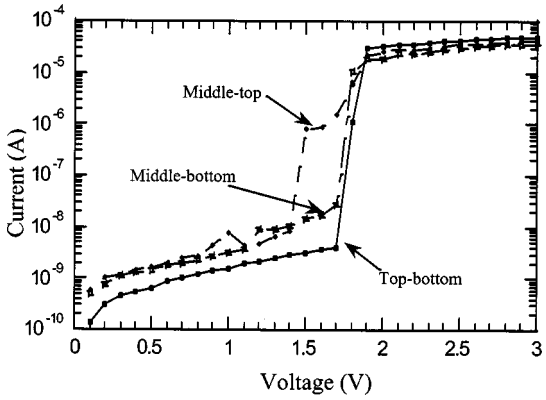

FIG. 10. The $I-V$ characteristics for a three-terminal OBD with no direct chemical reaction between Al and AIDCN at the top-Al/top-AIDCN interface. The top part and the bottom part have equal OFF-state resistance. Both parts show similar electrical bistability. Here, "middle-top," "middle-bottom," and "top-bottom" in the figure refer to the $I-V$ measurements done through the middle-top electrode, middle-bottom electrode, and the top-middle electrode, respectively.

bottom-AIDCN interface. On the other hand, the spectrum for hot Al deposited on top of an AIDCN layer shows significant differences compared with that of single AIDCN film, i.e., the AIDCN absorption peak at 326-nm wavelength is reduced by the deposition of hot Al, there is no clear absorption edge, and absorbance increases gradually from 700-nm wavelength, indicating gap-state formation. We also did the ultraviolet/x-ray photoelectron spectroscopy (UPS/XPS) study and found similar results (not shown here).

The large difference between R_{top} and R_{bottom} for devices at the OFF state can be understood in the following fashion. From the analysis above, we believe that there is a chemical reaction (or charge transfer) at the top-Al/top-AIDCN interface in which Al clusters lose partial electrons to AIDCN, forming a metal-organic complex [Fig. 9(a)]. This complex formation leads to gap-state formation as shown in Fig. 9(c), resulting in electrons that can easily inject from the top electrode into the organic layer, transport through the top-AIDCN layer, and jump off into the middle electrode layer without much energy loss. This electron injection and transportation process determines that the top part of the OBD has a relatively low resistance. On the other hand, the chemical reaction between the bottom AIDCN and the bottom Al is small [Fig. 9(b)], as a result, there is still a relatively larger energy barrier for electron injection from the bottom electrode as shown in Fig. 9(d). In addition, electrons injected from the top electrode also need more energy to overcome the energy barrier between the nanoclusters layer and the bottom AIDCN layer, resulting in a larger interfacial resistance at the nanocluster-layer/bottom-AIDCN layer. Hence, the applied potential to an OBD at the OFF state is mainly dropped on the bottom part of the device. When the device is switched ON, charges are stored at both sides of the nanoclusters layer,[16,17] which dynamically dopes the interfaces between the nanocluster layer and the two organic layers. As a result, the large interfacial resistance between the nanocluster layer and the bottom AIDCN layer is tremendously reduced. Alternatively, one can consider that the density of states (DOS) of organics increases tremendously, resulting in a several orders in magnitude change for R_{bottom} in the switching-on process as shown in Fig. 6. On the other hand, R_{top} shows a small jump at the switching voltage (shown in Fig. 6) since R_{top} is relatively small at the OFF state.

We can control the top-Al/top-AIDCN interface by introducing a small amount of oxygen during the first 5-nm top-Al electrode deposition to form an Al_2O_3 layer. This method will passivate the interface and prevent the direct charge transfer between Al and AIDCN, leading to a relatively high electron injection barrier at the top-electrode/top-AIDCN interface for the device at the OFF state. Hence, a very nice electrical bistability can be observed for both the top part and the bottom part of the OBD, as shown in Fig. 10, which may double the data storage capacity of OBDs. It should be noted that in Fig. 10, the measured current through the middle-top and middle-bottom electrodes is smaller than that through the top-bottom electrodes, which is caused by the resistance of the middle electrode of the three-terminal OBD.

It should be mentioned that the structure of the three-terminal OBDs is very promising in electronic devices, and can be generalized as a five-layer-stacked-structure device with three electrode layers. Recently, we demonstrated a vertical organic field-effect transistor, which is based on the OBD structure, where the bottom electrode acts as the gate electrode and the bottom organic layer is replaced with a dielectric layer.[19]

IV. CONCLUSION

We have demonstrated a three-terminal organic memory device by wiring out the metal-nanocluster layer of the organic electrical bistable device (OBD), which has a structure of organic/metal-nanocluster/organic trilayer sandwiched between a top and a bottom electrode. When the top part (top-electrode/top-organic/metal-nanocluster) and the bottom part (metal-nanocluster/organic/bottom-electrode) are not electrically the same, caused by interface formation, the potential difference of the middle electrode may be detected for a biased device (less than switching voltage) between the ON state and the OFF state. We have fabricated three-terminal OBDs with different potential distributions between the top and bottom parts by vacuum thermal evaporation method. The potential of the middle electrode changes from 0.2 mV

to 0.77 V when the whole device is switched from the OFF state to the ON state. The three-terminal OBDs can be read out by measuring the potential of the middle electrode, which is independent of the device area. Hence the reading of the three-terminal OBDs is still effective as the memory cell shrinks to micro- or submicro scale. It was also found that the electrical contact between the top-Al/top-AIDCN and the bottom-AIDCN/bottom-Al is different, which causes the two parts of the three-terminal OBDs to be electrically asymmetric and causes the tremendous increase of the potential of the middle electrode during the switching-on process. By preventing the direct chemical reaction at the top-Al/top-AIDCN interface, we also fabricated three-terminal OBDs showing nice electrical bistability for both the top part and the bottom part, which may double the memory capacity of the OBDs.

ACKNOWLEDGMENTS

The authors are indebted to the financial support from the Air Force Office of Scientific Research (Grant No. F49620-01-1-0427, program manager Dr. Charles Lee) and from the National Science Foundation (Grant No. DMR-0305111, Dr. LeVerne Hess).

[1] J. Campbell Scott, Science **304**, 62 (2004).
[2] J. Li, E. Schreck, and K. Dransfeld, Appl. Phys. A: Solids Surf. **53**, 457 (1991).
[3] R. S. Potember and T. O. Poehler, Appl. Phys. Lett. **34**, 407 (1979).
[4] H. Carchano, R. Lacoste, and Y. Segui, Appl. Phys. Lett. **19**, 414 (1971).
[5] H. K. Henish and W. R. Smith, Appl. Phys. Lett. **24**, 589 (1974).
[6] Y. Segui, B. Ai, and H. Carchano, J. Appl. Phys. **47**, 140 (1976).
[7] T. Oyamada, H. Tanaka, K. Matsushige, H. Sasabe, and C. Adachi, Appl. Phys. Lett. **83**, 1252 (2003).
[8] A. Bandyopadhyay and A. J. Pal, Appl. Phys. Lett. **82**, 1215 (2003).
[9] S. Moller, C. Perlov, W. Jackson, C. Taussig, and S. R. Forrest, Nature (London) **426**, 166 (2003).
[10] S. Moller, S. R. Forrest, C. Perlov, W. Jackson, and C. Taussig, J. Appl. Phys. **94**, 7811 (2003).
[11] L. P. Ma, Q. F. Xu, and Y. Yang, Appl. Phys. Lett. **84**, 4908 (2004).
[12] J. Ouyang, C. W. Chu, C. Szmanda, L. P. Ma, and Y. Yang, Nat. Mater. **3**, 918 (2004).
[13] L. P. Ma, J. Liu, S. M. Pyo, and Y. Yang, Appl. Phys. Lett. **80**, 362 (2002).
[14] L. P. Ma, J. Liu, and Y. Yang, Appl. Phys. Lett. **80**, 2997 (2002).
[15] L. P. Ma, J. Liu, S. M. Pyo, Q. F. Xu, and Y. Yang, Mol. Cryst. Liq. Cryst. Sci. Technol., Sect. A **378**, 185 (2002).
[16] L. P. Ma, S. M. Pyo, Q. F. Xu, and Y. Yang, Appl. Phys. Lett. **82**, 1419 (2003).
[17] J. H. Wu, L. P. Ma, and Y. Yang, Phys. Rev. B **69**, 115321 (2004).
[18] L. D. Bozano, B. W. Kean, V. R. Deline, J. R. Salem, and J. C. Scott, Appl. Phys. Lett. **26**, 607 (2004).
[19] L. P. Ma and Y. Yang, Appl. Phys. Lett. **85**, 5084 (2004).